Tropical Pacific 1976–77 Climate Shift in a Linear, Wind-Driven Model*

ALICIA R. KARSPECK AND MARK A. CANE

Lamont-Doherty Earth Observatory, Columbia University, Palisades, New York

(Manuscript received 5 September 2000, in final form 20 January 2002)

ABSTRACT

A number of studies have attempted to explain the cause of decadal variability in the tropical Pacific and explore its possible link to decadal variability in the midlatitude Pacific. To investigate some of the current theories of Pacific decadal variability, a linear, wind-driven model, designed to simulate only baroclinic wave dynamics, was forced with wind stress anomalies in the Pacific Ocean basin from 1945 through 1992. An analysis technique designed to isolate the decadal/interdecadal scale variability from interannual ENSO variability was performed on the model's thermocline depth anomaly (TDA).

It was found that the temporal and spatial patterns of the observed tropical decadal sea surface temperatures are consistent with our modeled TDA. Furthermore, restricting the wind forcing to within 5° of the equator does not substantially alter the decadal/interdecadal variability of the equatorial region. The authors conclude that the observed decadal variability in the low-latitude Pacific is primarily a linear dynamical response to tropical wind forcing and does not directly require an oceanic link to the midlatitudes. The question of how tropical wind anomalies are generated is not addressed.

In addition, it is shown that in model scenarios where the wind forcing is restricted to the western equatorial Pacific, the 1976–77 climate shift is still clearly visible as a dominant feature of tropical decadal variability. The temporal decadal signal of the model-generated TDA is more pronounced during the eastern equatorial upwelling season (July–September) than in the boreal winter. This is consistent with the observed seasonal bias in tracer and SST data from the eastern equatorial Pacific.

1. Introduction

There has been much debate regarding the cause of decadal-scale variability in the tropical Pacific Ocean. This low frequency variability has been characterized by changes in the frequency and intensity of ENSO events (e.g., Trenberth and Hoar 1996; Rajagopolan et al. 1997) as well as variations of the mean sea surface temperature (SST: Zhang et al. 1997; Tanimoto et al. 1993). The decadal variability of the North Pacific Ocean and atmosphere has also been well documented (Trenberth 1990; Graham 1994; Trenberth and Hurrell 1994). Many studies have addressed the possibility that the decadal fluctuations of the tropical Pacific are remotely driven by midlatitude dynamics.

The Luyten–Pedlosky–Stommel (LPS) theory of the ventilated thermocline (Luyten et al. 1983) provides a physical mechanism by which SST anomalies generated in the midlatitudes can subduct and advect equatorward along surfaces of constant density. In the context of the LPS theory, the equatorial thermocline is composed of these remotely outcropping isopycnals. Thermal anomalies that arrive from the midlatitudes at the equator are swept eastward by the Equatorial Under-current, a swift subsurface current that flows inside the thermocline, confined to within 2° of the equator. In the eastern equatorial Pacific the thermocline shoals to the surface, exposing its layers to the tropical atmosphere. These waters can then return to the subtropics via surface Ekman drift. Tracer studies (e.g., Fine et al. 1987) and ocean general circulation models (e.g., Liu et al. 1994) support the existence of this subtropical circulation cell. Variations in the eastern equatorial SST can then readily influence tropical (and extratropical) atmospheric winds, positively reinforcing the initial thermal anomaly. The timescale of the oscillation is set by the advective travel time of the anomalies from the midlatitudes to the Tropics—approximately a decade.

The observational study of Deser et al. (1996) tracked the advection of a cold subsurface anomaly as it propagated equatorward from the eastern North Pacific in the late 1970s and 1980s. Zhang et al. (1998) have attributed the tropical warming of 1976–77 to the arrival of a warm anomaly from the midlatitudes. Gu and Philander (1997) constructed a simple model of a tropical–midlatitude decadal climate oscillation based on an oceanic advective bridge between the two regions. How-

* Lamont-Doherty Earth Observatory Contribution Number 6288.

Corresponding author address: Alicia R. Karspeck, Lamont-Doherty Earth Observatory, 103 Oceanography, Box 1000, Palisades, NY 10964.
E-mail: aliciak@ldeo.columbia.edu

ever, subsequent studies have demonstrated that subducted thermal anomalies from the midlatitudes peter out at the poleward edge of the Tropics and that local wind forcing is predominately responsible for the decadal-scale variability in the low latitudes (Schneider et al. 1999a, 1999b; Hazeleger et al. 2001).

An alternative oceanic bridge was examined by Lysne et al. (1997). They found that wave propagation of midlatitude forced anomalies could result in decadal modulation of the tropical thermocline. Their connection consisted of midlatitude thermal anomalies that propagate to the western boundary via long Rossby waves and travel equatorward as coastal Kelvin waves. However, they note that the magnitude of the decadal variations are small compared with observations and that local equatorial processes may have a significant impact on the low frequency variability.

An atmospheric link between the midlatitudes and Tropics on decadal timescales has also been studied (Wang and Weisberg 1998; Barnett et al. 1999)—most recently with a coupled global circulation model by Pierce et al. (2000). The contention is that decadal wind anomalies generated in the midlatitudes extend far enough into the Tropics to influence equatorial dynamics. An advantage of the atmospheric bridge concept is that it allows the connection between the midlatitudes and Tropics to be nearly instantaneous, an aspect of Pacific decadal variability that is supported by the observational record.

The possibility also exists that decadal variability in the tropical Pacific is locally generated and drives midlatitude decadal variability through an atmospheric link. Still another option is that decadal variability is generated outside the Pacific and simultaneously influences both the Pacific Tropics and midlatitudes. While there is general agreement that interannual ENSO variability originates in the Tropics, there is no consensus about the origin of decadal-scale variability.

We focus on the 1976 climate shift in the tropical Pacific as the dominant feature of decadal variability. The purpose of this study is to illustrate the theoretical possibility that the observed shift in tropical SST in 1976 can be generated soley through tropical wind-driven, linear waves traveling through the thermocline. We examine this idea through the framework of a simple ocean model capable of resolving only linear baroclinic wave dynamics. This model is essentially the solution to the linear shallow-water equations on an equatorial β plane forced with observed wind stress.

The utility in using such an idealized model is that it allows us to eliminate the possibility of advecting thermal anomalies from the midlatitudes. More generally, a theoretical model such as this simplifies the interpretation of our results: all of the model-generated tropical variability is a linear planetary wave response to either local or remote wind stress forcing.

A comprehensive explanation of the source and mechanism of the 1976 climate shift would require making an explicit physical link to tropical SST because it is through this oceanic variable that the atmosphere couples to the ocean. However, our analysis focuses on model-generated thermocline depth anomalies (TDA) instead. We have made the implicit assumption that tropical SST variations are highly sensitive to changes in thermocline depth. This assumption forms the basis of the relevance of this study. In fact, it should be considered that all of the theories put forth on the source of Pacific decadal variability rely on the validity of this assumption.

The following two sections describe the linear model that was used in this study and present the wind stress and SST datasets. In section 4 we use an analysis like that of Zhang et al. (1997) to isolate the decadal variability in our model results. These results are compared to SST data subjected to a comparable analysis. In section 5 we restrict the wind forcing to within the tropical model domain in order to determine how much of the tropical decadal variability is locally forced. We also present the results of a model scenario in which wind forcing was applied only in the western equatorial Pacific. In section 6 we present the model results sorted by season to demonstrate that the tropical decadal variability has a seasonal bias. The conclusions are discussed in section 7.

2. The linear, wind-driven ocean model

The nondimensional linear shallow-water equations on an equatorial β plane can be written as

$$\partial_t u - yv + \partial_x h = \tau_x,$$

$$\partial_t v + yu + \partial_y h = \tau_y,$$

$$\partial_t h + \partial_x u + \partial_y v = 0.$$

Here u and v are the zonal and meridional velocity perturbations, respectively; h is the layer depth perturbation; and τ_x and τ_y are the prescribed zonal and meridional components of the wind stress. The dimensional variables can be recovered by multiplying h by H, u and v by U, t by T, and x and y by L. The dimensional forcing terms are $\tau(U/T)$. The scales are given by $U = c$, $H = c^2/g$, $L = (c/\beta)^{1/2}$, and $T = (c\beta)^{-1/2}$, where β is the variation of the coriolis parameter with latitude, given by $\partial f/\partial y|_{y=0}$; c is the wave phase speed (discussed below); and g is the gravitational acceleration.

The shallow-water system is solved for two vertically standing normal modes, with speeds $c_1 = 2.98$ m s^{-1} and $c_2 = 1.84$ m s^{-1} for baroclinic modes one and two, respectively. These wave speeds are calculated from the observed vertical density profile taken on the equator at the date line (Levitus and Boyer 1994) and are assumed to be uniform over the entire domain. The resultant thermocline depth anomalies are given as the linear combination of modes one and two.

The shallow-water equations were solved using a numeric scheme developed by Israeli et al. (2000) called

INC. It is a hybrid of semi-Lagrangian methods and the Cane and Patton (1984) scheme. In the INC scheme the zonal part of the wave operator is isolated and used to find the values of u and h in terms of v and known quantities at the next time step using a semi-Lagrangian, explicit technique. The meridional velocity, v, is then solved implicitly, as in the Cane–Patton scheme. As with semi-Lagrangian and Cane–Patton, the time step in the INC scheme is not limited by a CFL condition. Unlike Cane–Patton, the INC scheme is able to handle irregular, realistic coastal geometry. The time step used in the model is 20.73 h and the spatial resolution is 2° zonally and ½° meridionaly. With the exception of a closed Indonesian Throughflow and the absence of the island of New Guinea, realistic coastlines bound the model domain to the east and west. Meridional boundaries extend to 60°N/S.

3. Data

Monthly da Silva et al. (1994) wind stress anomalies were used to force the model in the Pacific Ocean basin in the years 1945–92. The wind stress data fields are on a 1° lat by 1° lon grid.

All of the SST data used for our analysis were based on the Comprehensive Ocean–Atmosphere Data Set (COADS) subjected to an objective analysis by da Silva et al. (1994). The climatological mean for each month, based on the period 1945–92, was subtracted from the data to obtain monthly SST anomalies. Both TDA model output and SST data were interpolated onto identical 2° (zonal) by 1° (meridional) grids so that their spatial patterns could be quantitatively compared. All analysis techniques were restricted to the Tropics, from 20°N to 20°S, where the model is known to give reasonable thermocline depths.

4. Total-basin-forcing scenario

ENSO is the dominant mode of variability in the Pacific. It is characterized in the ocean by anomalously warm (cool) SST in the eastern tropical Pacific, accompanied by anomalously cool (warm) SST in the north Pacific. While ENSO has representation over a wide range of frequencies, it is traditionally considered an interannual phenomenon, with greatest power in the 2–7-yr bands.

The studies of Tanimoto et al. (1993) and Zhang et al. (1996, 1997) first explored the possibility that ENSO variability could have a distinct decadal component. The difficulty in isolating the decadal variability stems from its spatial similarity to the interannual ENSO signal (hereafter referred to as ENSO). Indeed, conventional EOF analysis of the data fields in the Pacific will not yield separate decadal and interannual modes (Zhang et al. 1997).

In order to isolate the decadal variability, following Zhang et al. (1997), we calculated the leading principal component (PC) of the TDA decadal residual as follows: 1) Monthly SST data from the Niño-3 region (5°N/S, 90°–150°W) was spatially averaged in the years 1945–92. A 6-yr high-pass Butterworth filter was applied to this time series to strip it of variability on time periods longer than interannual. We use this as an index to represent interannual ENSO variability, and it will be referred to as the ''ENSO index'' (Fig. 1, top panel). 2) The model-generated TDA fields between 20°N and 20°S were regressed upon the ENSO index. These regression coefficients were used to obtain a fitted time series at each point, which was then subtracted from the original TDA. The assumption we have made here is that, on ENSO timescales, the relationship between SST in the Niño-3 region and TDA in the entire tropics is linear. The TDA fields that have had the ENSO index removed will be called the TDA decadal residual, and more accurately, the ''ENSO-free'' TDA. 3) The leading PC of this residual field was then calculated. The associated spatial pattern is the regression of the original TDA field onto the leading PC of the decadal residual. Note that this pattern is not strictly the first EOF because the PC is the leading temporal pattern of the decadal residual, not the unfiltered TDA. The leading PC of the decadal residual of the tropical SST fields was also calculated with an identical procedure.

The temporal pattern of the decadal residual shows significant high frequency variability. This is not surprising considering that our technique for generating a decadal residual does not involve any smoothing of the SST or TDA fields.

The leading PC of the TDA decadal residual exhibits low frequency variability that is qualitatively similar to the first PC of the SST decadal residual (Figs. 2 and 3, top panels). They are correlated at an r value of 0.53. (This is significant at a greater than 99% confidence level.) If a 72-month low-pass Butterworth filter is used to smooth the high frequencies out of the two PCs, the correlation coefficient is 0.67 (with degrees of freedom reduced to 8, this r is significant at the 95% confidence level).

The eastern equatorial thermocline gradually shoals from the late 1960s until 1976, when it abruptly deepens and remains deep until the late 1980s. An anomalously deep thermocline in the eastern equatorial Pacific is consistent with warmer SST because less cool thermocline water shoals to the surface. The abrupt shift in 1976 is the dominant feature of decadal variability in this time series. This climate shift is characterized in the observations by the abrupt warming of tropical SST following the 1975 La Niña event, and the persistence of warm temperatures for over a decade.

The regression patterns of the leading PCs of the TDA and SST decadal residual are physically consistent with one another. Although SST is strongly influenced by the depth of the thermocline below it, we would not expect the spatial structure of SST and TDA to be identical. The eastern equatorial Pacific is a region of vigorous

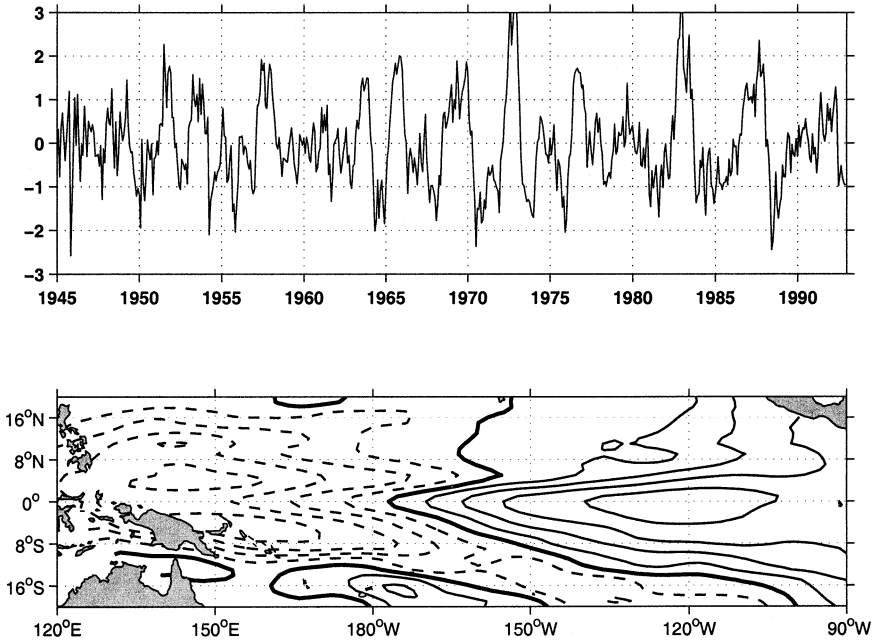

FIG. 1. The top panel is the average SST in the Niño-3 region. A 6-yr high-pass filter has been applied to remove any decadal or interdecadal variability. We have defined this resulting time series as the index of interannual ENSO variability (in units of standard deviations). The bottom panel shows the regression pattern of the model generated TDA onto the ENSO index. The contour interval is 1 m per std dev of the ENSO index. The bold contour is the zero line, solid contours are positive, and dashed contours are negative.

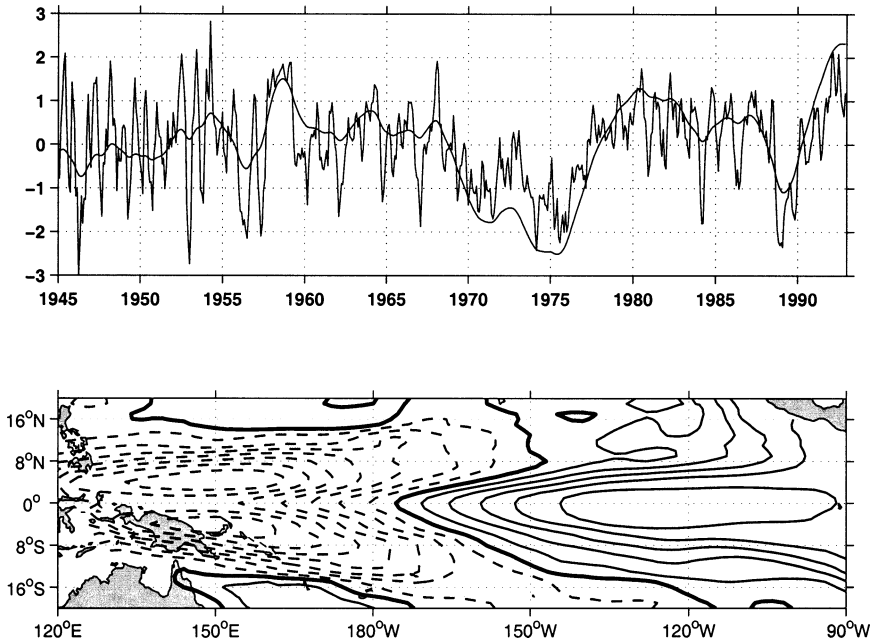

FIG. 2. The top panel depicts the leading (normalized) PC of the TDA decadal residual. ENSO-scale variability was removed from the TDA fields by subtracting the ''best fit'' linear regression of the ENSO index. The lower-frequency overlay is the leading PC of the 72-month low-pass filtered ENSO-free TDA field (independently normalized). The bottom panel shows the associated regression pattern of the TDA field onto the PC. The time series is in units of standard deviations, and the contours of the spatial pattern are 1 m per std dev of the PC. Contouring conventions are as described in Fig. 1.

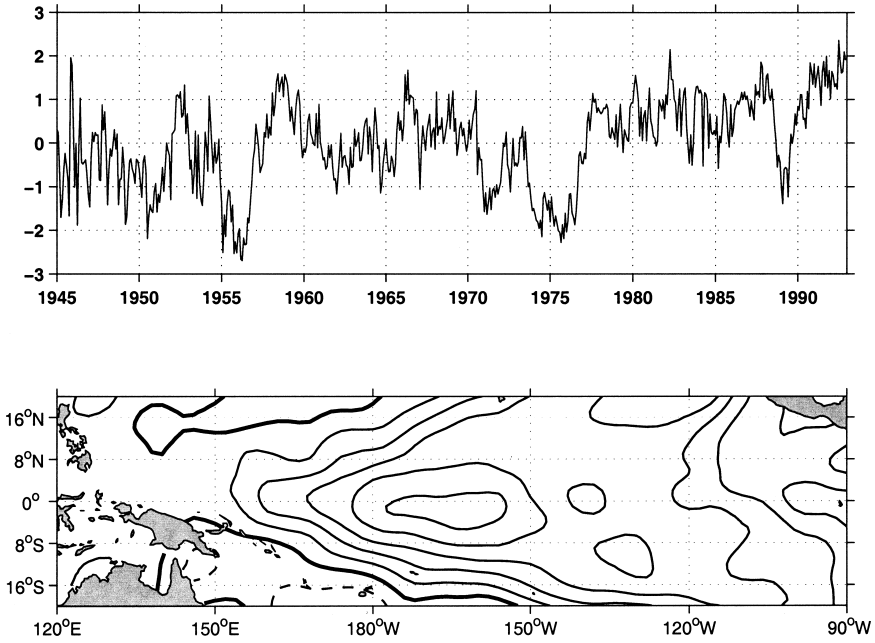

FIG. 3. (top panel) The leading (normalized) PC of the SST decadal residual. ENSO-scale variability was removed from the SST fields by subtracting the ''best fit'' linear regression of the ENSO index. (bottom panel) The associated regression pattern of the observed SST fields onto the SST decadal residual time series. The PC is in units of standard deviations and the regression pattern has contour intervals of 0.1°C per std dev of the PC. Positive contours are solid lines and the zero contour is bold.

upwelling, where the thermocline is within 50 m of the ocean surface. It is in this region that the SST is most sensitive to changes in the depth of the thermocline. In the western equatorial Pacific, where the mean depth of the thermocline is far below the surface, the SST does not respond as dramatically to small changes in the TDA and is dominated by other ocean and atmospheric processes. The two distinct off-equatorial lobes of the TDA regression pattern in the western equatorial Pacific are representative of locally forced Rossby waves (Fig. 2, bottom panel).

The TDA decadal residual regression pattern is similar to the interannual ENSO spatial pattern. Figure 1 (bottom panel) shows the regression of the TDA fields upon the ENSO index (defined in the previous section). The spatial correlation coefficient between the interannual and the decadal residual regression patterns (Figs. 1 and 2, lower panels) is extremely high, with an r value of 0.93.

It has been suggested that this familiar ''see-saw'' spatial pattern of the TDA could be generated by regression of the full field TDA upon *any* high-frequency, variable time series. We tested this idea by generating an AR(1) model of the first PC of the decadal residual and regressing these same TDA fields upon it. The resulting spatial pattern (not shown), while of opposite sign in the east and west equatorial Pacific, does not exhibit the strength or distinct structures that we associate with the ENSO and decadal-ENSO TDA pattern.

While in the ENSO regression pattern (Fig. 1) the response in the eastern and western equatorial Pacific are of similar magnitude, in the decadal residual spatial pattern (Fig. 2) the magnitude of the TDA response in the west is greater than that in the east. This suggests that, in addition to a tilting of the equatorial thermocline, there may also be changes in the zonal mean depth. Figure 4 shows the difference and sum of the ENSO-free TDA in the warm pool of the western equatorial Pacific (5°N/S, 120°E–180°) and the Niño-3 region. The difference is defined as $\frac{1}{2}(\mathrm{TDA}_{\mathrm{nino}} - \mathrm{TDA}_{\mathrm{wp}})$ and the sum as $\frac{1}{2}(\mathrm{TDA}_{\mathrm{nino}} + \mathrm{TDA}_{\mathrm{wp}})$. The tilting, or difference, shows the familiar 1976–77 shift. Although less pronounced, the zonal mean thermocline depth over the entire equatorial region exhibits a shift toward a shallower thermocline after the mid 1970s. Both of these shifts are statistically significant at the 90% confidence level.

The ENSO-free TDA difference field between the epochs January 1960–August 1976 and August 1977–December 1992 is similar to the TDA decadal residual regression pattern (Fig. 5). When the decadal residual PC analysis is restricted to either the first or the second epoch, the same spatial regression pattern is manifest. This shows that the decadal pattern is not just a reflection of the 1976–77 shift. The changes that took place in 1976 are spatially representive of the decadal pattern.

The existence of a tropical decadal pattern in these TDA fields that is spatially and temporally consistent

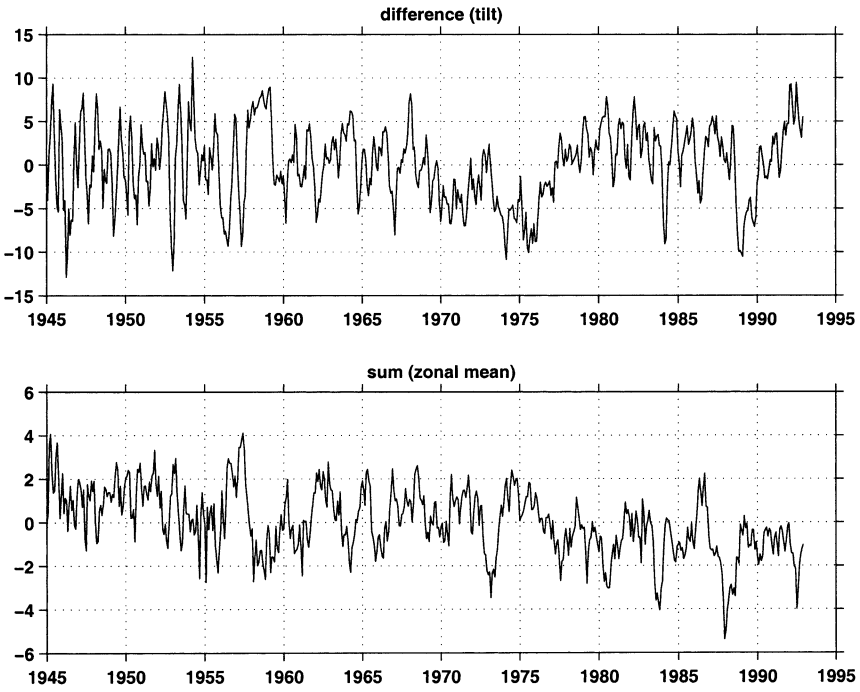

FIG. 4. The difference and sum of the TDA in the Niño-3 region (5°N/S, 90°–150°W) and the western warm pool (5°N/S, 120°E–180°) of the equatorial Pacific. The difference is defined as $\frac{1}{2}(\mathrm{TDA}_{\mathrm{nino}} - \mathrm{TDA}_{\mathrm{wp}})$ and represents the tilt of the equatorial thermocline. Units are in meters. The sum is defined as $\frac{1}{2}(\mathrm{TDA}_{\mathrm{nino}} + \mathrm{TDA}_{\mathrm{wp}})$ and represents zonal mean changes in the depth of the equatorial thermocline.

with SST data suggests that tropical oceanic decadal variability, to a first-order approximation, can be explained by linear baroclinic wave dynamics. However, this does not exclude the (unlikely) possibility that advected thermal anomalies from the midlatitudes, initially small thermocline perturbations, could trigger large-scale tropical wind variations that feedback into significant changes in thermocline depth (see Gu and Philander 1997).

5. Wind forcing restricted to within the Tropics

In order to determine how much of this TDA decadal residual pattern is driven by local, tropical winds, we performed additional model runs. The wind stress forcing was restricted to within 12°N/S, 10°N/S, 7°N/S, and 5°N/S (hereafter referred to as F_{12}, F_{10}, F_7, and F_5). The original run, in which the entire model domain is forced with wind stress is denoted F_{total}. A mask with zeros poleward of the forcing limits and ones in the forcing region was applied to the wind stress anomaly fields. To reduce spurious wind stress curl, the poleward edges of the mask were tapered by applying two passes of a 1–2–1 filter prior to multiplication with the wind fields.

For each scenario the decadal residual was calculated as outlined in section 3. The resulting PCs and associated regression patterns are shown in Fig. 6. The PCs are nearly indistinguishable from the full-basin-forced

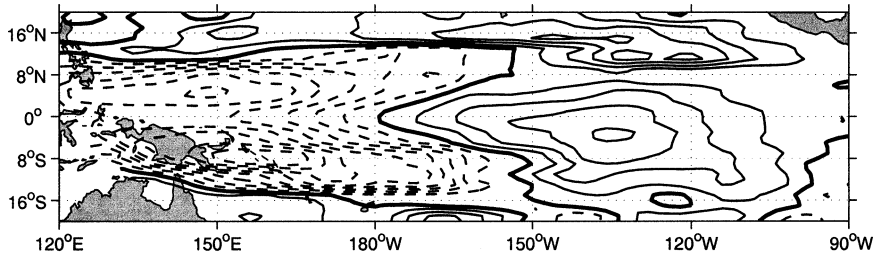

FIG. 5. A difference map of the temporal means of the ENSO-free TDA fields before and after the 1976–77 climate shift. The epoch prior to the shift extended from Jan 1960 to Aug 1976. The second epoch was defined from Aug 1977 to Dec 1992. This difference pattern is similar in structure to the regression pattern associated with the decadal residual. Contour intervals are 1 m and contouring conventions are described in Fig. 1.

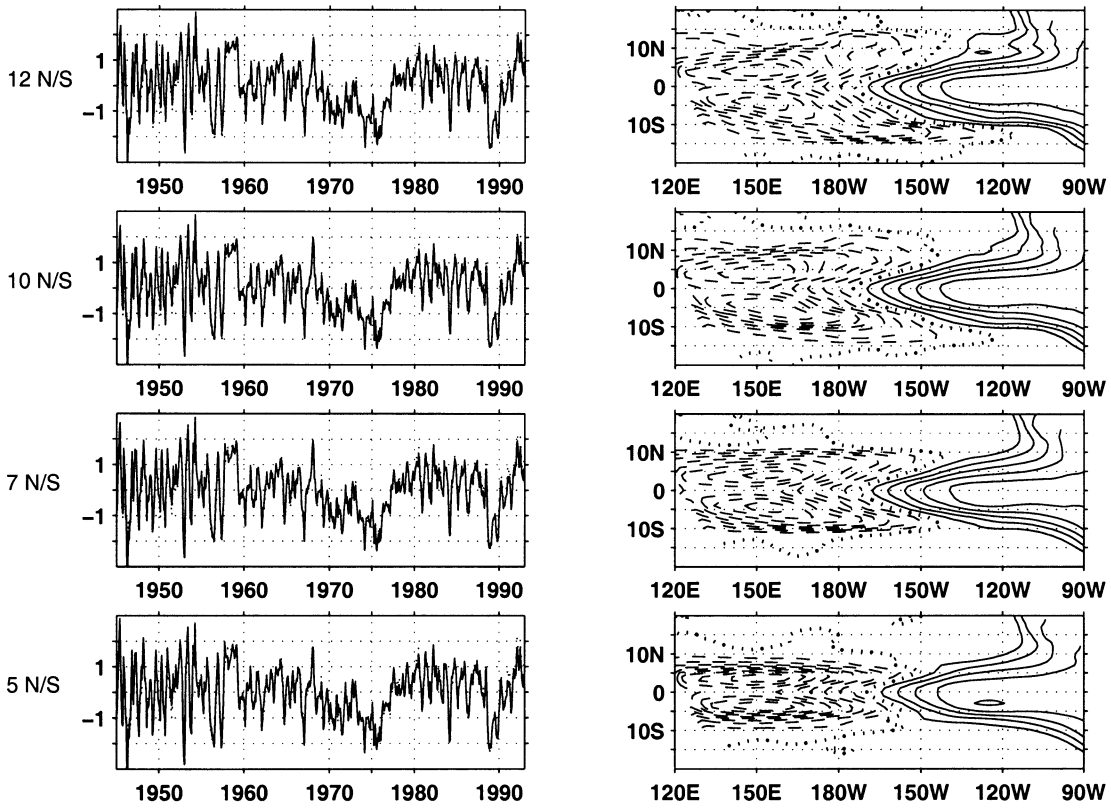

FIG. 6. (from top to bottom) Decadal residual analysis (described in text) applied to model scenarios where wind forcing was restricted to between 12°, 10°, 7°, and 5°N/S. The PC of F_{total} is the dotted overlay. (left panels) The leading (normalized) PCs of the decadal residuals and (right panels) the associated regression patterns of the TDA fields. Tick marks in the left panels are equal to one standard deviation. The regression patterns have contour intervals of 1 m per std dev of the PC time series. Negative contours are dashed and zero contour is thickened.

model scenario, and the abrupt shift in 1976 remains clearly visible. The PCs are correlated with the full-basin-forced PC at values of $r = 0.987$ (F_{12}), $r = 0.989$ (F_{10}), $r = 0.983$ (F_7), and $r = 0.977$ (F_5), and are similar in amplitude. The associated regression patterns are more reflective of the restricted forcing. In the western equatorial Pacific, where the thermocline response is largely driven by the local winds, the Rossby wave pattern is isolated to the region of wind forcing. In contrast, the eastern equatorial thermocline response retains its poleward width, extending beyond the forcing limits. This can be understood by considering that the thermocline response on the eastern equator is composed primarily of equatorial Kelvin waves generated in the western Tropics. The patterns' breadth about the equator is the poleward propagation of these disturbances as coastal Kelvin waves and their westward return as Rossby waves.

Lysne et al. (1997) concluded that midlatitude anomalies propagate into the Tropics by planetary waves. Figure 7 shows the results of a model scenario in which forcing was applied only poleward of 30°N/S. (Forcing was tapered as described above to avoid spurious wind stress curls). Time series of the average (normalized) TDA in the Niño-3 and warm pool regions are plotted in the upper panel. The associated regression pattern is shown below. The equatorial response to extratropical forcing is zonally uniform, as expected from linear wave theory (Cane and Moore 1981).

The details of the temporal signal are not accurate because our model uses a spatially uniform wave speed based on tropical stratification. The relevant aspect of this figure is the *magnitude* of the tropical TDA response to extratropical wind forcing. This remote wind forcing makes up less than 5% of the total ENSO-free, tropical TDA magnitude in the Niño-3 region. The thermocline's response to local forcing swamps the response to remote, extratropical forcing. It is unlikely that remotely forced waves propagating from the midlatitudes are able to coherently impact tropical dynamics, as they have a magnitude that is indistinguishable from noise.

The thermocline variations in the eastern equatorial region are in large part the Kelvin wave response to wind forcing in the west. We expect the western thermocline response to western equatorial wind forcing to be 180° out of phase with the thermocline response in the eastern equatorial Pacific. This can be understood by noting that the travel time of a Kelvin wave crossing

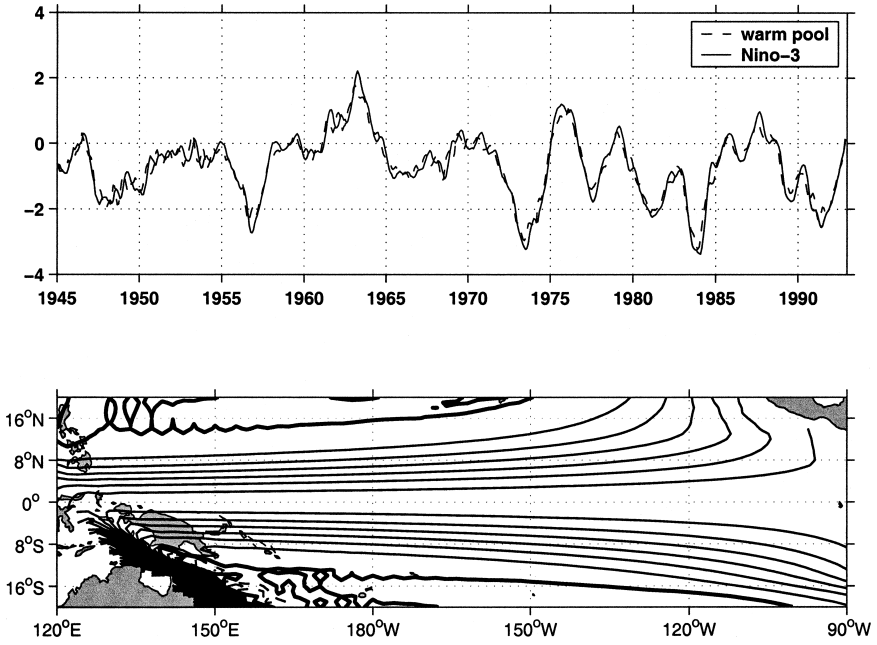

FIG. 7. (top panel) Average (normalized) TDA in Niño-3 and warm pool regions, taken from modeling scenario where wind forcing was applied only poleward of 30°N/S. Time series are in units of standard deviations. (bottom panel) Regression of TDA onto the Niño-3 time series shown in the top panel. Contour interval is 0.02 m per std dev of the time series. Negative contours are dashed and zero contour is bold.

the equatorial Pacific is approximately 2 months, shorter than the timescales of the major forcing fluctuations. So, a significant portion of the response in the eastern equatorial Pacific is the result of Kelvin wave packets traveling eastward along the equator. This mechanism for quickly transmitting information across the basin does not exist for waves originating in the east. Eastern generated waves must travel poleward along the coast of the Americas as coastal Kelvin waves and return to the west via the slower Rossby wave.

To test the idea that the 1976–77 TDA shift in the east has its origins in the western equatorial wind forcing, the model was forced with wind stress only in the western equatorial Pacific (5°N/S, from 120°E to 170°W). Forcing fields were tapered (by applying two passes of a 1–2–1 filter) to avoid strong wind stress curls. Figure 8 depicts the first PC of the decadal residual for this scenario and the associated regression pattern. The first PC exhibits the same gross temporal structure as in the F_{total} scenario, with a clear jump in 1976. As we would expect, the spatial regression pattern in the western Pacific Ocean is extremely similar to the F_5 spatial pattern. The waves that are excited in this region are forced by wind stress in the immediate vicinity. As we expect from theory, there is also a strong eastern Pacific signature. It is more equatorially trapped than in F_{total} and it is of a slightly lower magnitude, but it is similar in structure. This result suggests that the 1976 shift is primarily driven by western equatorial Pacific winds.

6. Seasonal bias of decadal variability

Guilderson and Schrag (1998, hereafter GS) presented chemical tracer evidence for a seasonal bias to the 1976–77 tropical climate shift. They analyzed $\Delta^{14}C$ data from Galapagos Island coral from 1957 to 1982 in conjunction with SST data from the Niño-3 region from the years 1956–1992.

Through air–sea exchange processes, the atmospheric $\Delta^{14}C$ can enrich the ocean surface waters, while deeper waters maintain relatively low concentrations. In regions of vigorous upwelling like the Galapagos Islands, surface $\Delta^{14}C$ concentrations are sensitive to the influx of radiocarbon depleted waters from the ocean depths.

The upwelling of waters in the eastern equatorial Pacific is a seasonal phenomenon, driven by climatological variations in the strength of the trade winds. During the upwelling season (July–September), the easterly trade winds strengthen, increasing the east/west tilt of the equatorial thermocline. Cool, radiocarbon depleted water from the thermocline is then available to upwell into the eastern equatorial mixed layer.

The seasonal cycle of the eastern upwelling is reflected in both the surface $\Delta^{14}C$ record and the SST record. The expectation is that the $\Delta^{14}C$ content of the surface waters will be lowest during the upwelling season and highest when the eastern thermocline is deep below the surface. Similarly, the SST is at a minimum during the upwelling season and peaks in January–March.

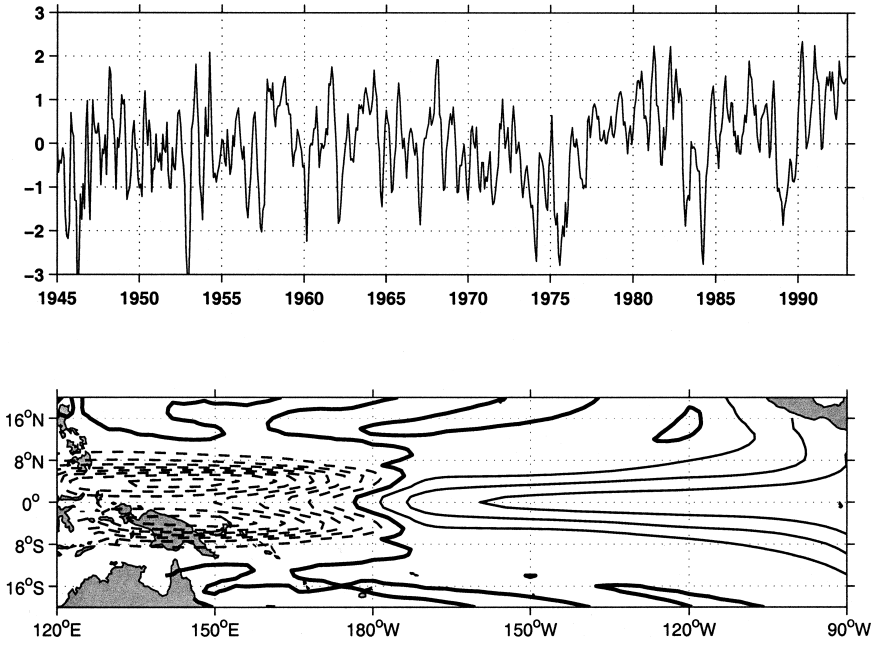

FIG. 8. Decadal residual analysis (described in text) applied to model scenario where wind forcing was restricted to the western equatorial Pacific. Tick marks in the top panel are 1 std dev. The regression pattern has contour intervals of 1 m per std dev of the associated PC series. Negative contours are dashed and zero contour is thickened.

In their analysis of the $\Delta^{14}C$ record, GS found that the amplitude of the seasonal cycle decreased after 1976. (They excluded the strong El Niño years from their analysis in an attempt to define the shift as separate from variations in ENSO.) The decrease in the cycle amplitude was caused by an abrupt increase in the annual minimum radiocarbon values. The timing of the abrupt shift in $\Delta^{14}C$ concentrations corresponds to the 1976–77 climate shift. Guilderson and Schrag note that the 1976–77 increase in eastern equatorial SST also has a seasonal bias.

The simultaneous shift in both the SST and radiocarbon records and its restriction to the upwelling season implies that in the years after 1976 the late boreal summer thermocline lay deeper below the surface in the eastern equatorial Pacific. An anomalously deep thermocline would reduce the upwelling of cool, radiocarbon depleted water, resulting in a surface layer that is warmer and more enriched with $\Delta^{14}C$ during the upwelling season.

Zhang et al. (1998) suggest that the warming of the eastern SST could be explained by the advection of a thermal anomaly from the North Pacific. However, this thermal advection hypothesis cannot explain the shift in the $\Delta^{14}C$ record because there is no reason that a radiocarbon high would accompany a thermal anomaly.

In order to test whether there is a seasonal bias to the first PC of the TDA decadal residual, we extracted and averaged the three upwelling months (July, August, and September) from each year. The top panel of Fig. 9 shows the upwelling season average of the modeled TDA (one point per year, plotted in time at January) and the lower panel shows the winter average (December, January, February). The familiar decadal temporal structure is evident in the upwelling season average, with a gradual shallowing from the 1960s into the 1970s and an abrupt and extended deepening after 1976. The structure is less obvious in the wintertime record.

As means of assessing the objectivity of this statement, we found that the average of the upwelling months before and after 1976 was significantly different at the 98% confidence level. The wintertime months, on the other hand, showed a difference in means that was significant at only the 28% confidence level.

This suggests that the wind-driven shift of 1976–77, as well as the other decadal structure of the time series, is more pronounced during the late northern summer upwelling season. This finding is consistent with the radiocarbon as well as the SST records in the eastern equatorial Pacific.

One possible explanation for the seasonal bias in the 1976–77 shift is that the decadal variability is less corrupted by the ENSO signal during boreal summer because ENSO events have not reached maturity. The regression technique that was used in this study to remove the ENSO signal could leave behind some high variance in the winter months, when ENSO peaks.

7. Conclusions

We have investigated the temporal and spatial patterns of decadal variability in the tropical Pacific ocean using

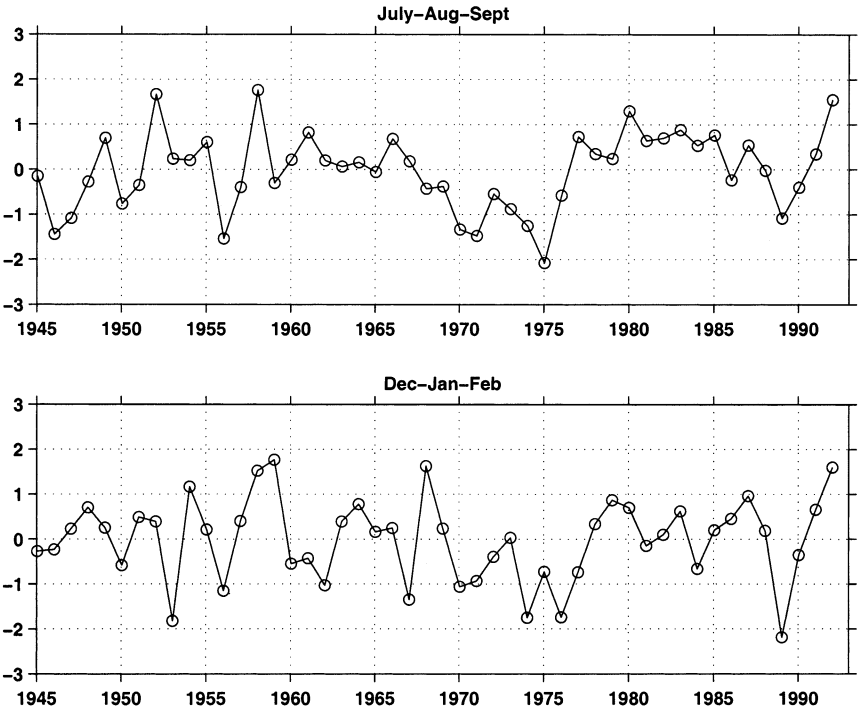

FIG. 9. The first PC of the ENSO-free TDA sorted and averaged into northern summertime and wintertime bins. The vertical axis is in units of standard deviations of thermocline depth anomaly (see bottom panel of Fig. 2 for depth scale). The decadal pattern is most evident in Jul–Aug–Sep, which corresponds to the eastern equatorial upwelling season. The average of the upwelling months before and after 1976 is significantly different at the 98% confidence level.

a linear, wind-driven model. Our model is capable of simulating only linear baroclinic wave dynamics, eliminating the possibility of advecting thermal anomalies from the midlatitudes into the Tropics. The purpose of this study was to compare the thermocline depth anomaly results from this model to SST data and to assess their consistency. We attempted to explore the effectiveness of linear, wind-driven planetary ocean waves at generating decadal variability that is consistent with the tropical SST observations, specifically focusing on the 1976–77 climate shift. Our conclusions are as follows:

1) The leading PC of the model generated tropical TDA decadal residual is physically consistent with the leading PC of the SST decadal residual as calculated by Zhang et al. (1997). The associated regression patterns are in good agreement in the eastern Tropics, where SST anomalies are sensitive to the depth of the thermocline. The dominant temporal features of the decadal variability, including the 1976–77 climate shift, are apparent in the modeled TDA, suggesting that tropical decadal variability in the ocean is largely a function of wind forcing. We do not address the question of what causes the decadal variability in the winds. This modeling study cannot thoroughly rule out the possibility of oceanic advection of anomalies along isopycnals as a midlatitude–tropical bridge. But it does suggest that, to play that role, the advected anomalies must influence the wind stress fields. There are no plausible suggestions as to how this might happen. A more likely midlatitude–tropical bridge is through the atmosphere.
2) The first PC of the TDA decadal residual in the model simulations where wind forcing was restricted to the Tropics (F_5 through F_{12}) correlate well with the full-basin-forced TDA decadal residual. Even when the forcing is restricted to within 5° north and south of the equator (F_5), the leading PC of the decadal residual correlates at $r = 0.977$. This finding rules out the possibility of midlatitude forced waves propagating into the Tropics as a direct mechanism for decadal variability. While there is evidence of midlatitude–tropical wave propagation, its amplitude at the equator is overwhelmed by the response to tropical wind forcing. This supports the conclusions of Schneider et al. (1999a,b) and Pierce et al. (2000), who also find that tropical variability is primarily forced by tropical winds.
3) The structure of the annual upwelling season average of the first PC of the ENSO-free TDA is more coherent than the wintertime average structure. Our analysis, along with the results of Guilderson and Schrag (1998), suggests that the decadal variability in the eastern tropical Pacific has the greatest ex-

pression during the late Boreal summer. The observed upwelling season variability in the tracer and SST records are due predominantly to the variability of the wind-driven thermocline.

Acknowledgements. Great thanks to Naomi Naik for assistance in running the INC model; Jeffrey Shaman for his patience, attention, and advice; and Donna Witter for her encouragement and support. The insight gained through interactions at the March 2000 ENSO conference and NCAR Summer Colloquium, 2000 has proved invaluable. Support for this research was provided by the National Science Foundation under Grant OCE 9819538 and ATM 9986072.

REFERENCES

Barnett, T., D. Pierce, M. Latif, D. Dommenget, and R. Saravanan, 1999: Interdecadal interactions between tropics and midlatitudes in the Pacific Basin. *Geophys. Res. Lett.,* **26,** 615–618.

Cane, M., and D. Moore, 1981: A note on low frequency equatorial basin modes. *J. Phys. Oceanogr.,* **11,** 1578–1584.

——, and R. Patton, 1984: A numerical model for low-frequency equatorial dynamics. *J. Phys. Oceanogr.,* **14,** 1853–1863.

da Silva, A., A. Young, and S. Levitus, 1994: *Algorithms and Procedures.* Vol. 1, *Atlas of surface marine data 1994.* NOAA Tech. Rep. SMD94, 83 pp.

Deser, C., M. Alexander, and M. Timlin, 1996: Upper-ocean thermal variations in the North Pacific during 1970–1991. *J. Climate,* **9,** 1840–1855.

Fine, R., W. Peterson, and H. Ostlund, 1987: The penetration of tritium into the tropical Pacific. *J. Phys. Oceanogr.,* **17,** 553–564.

Graham, N., 1994: Decadal-scale climate variability in the tropical and North Pacific during the 1970s and 1980s: Observations and model results. *Climate Dyn.,* **10,** 135–162.

Gu, D., and S. G. H. Philander, 1997: Interdecadal climate fluctuations that depend on exchanges between the tropics and the extratropics. *Science,* **275,** 805–807.

Guilderson, T., and D. Schrag, 1998: Abrupt shift in subsurface temperatures in the tropical Pacific associated with changes in El Niño. *Science,* **281,** 240–243.

Hazeleger, W., M. Visbeck, M. Cane, A. Karspeck, and N. Naik, 2001: Decadal upper ocean temperature variability in the tropical and subtropical Pacific. *J. Geophys. Res.,* **106C,** 8971–8988.

Israeli, M., N. Naik, and M. Cane, 2000: An unconditionally stable scheme for the shallow water equations. *Mon. Wea. Rev.,* **128,** 810–823.

Levitus, S., and T. P. Boyer, 1994: *Temperature*. Vol. 4, *World Ocean Atlas 1994,* NOAA Atlas NESDIS 4, 117 pp.

Liu, Z., S. G. H. Philander, and R. C. Pacanowski, 1994: A GCM study of tropical–subtropical upper-ocean water exchange. *J. Phys. Oceanogr.,* **24,** 2606–2623.

Luyten, J., J. Pedlosky, and H. Stommel, 1983: The ventilated thermocline. *J. Phys. Oceanogr.,* **13,** 292–309.

Lysne, J., P. Chang, and B. Giese, 1997: Impact of the extratropical Pacific on equatorial variability. *Geophys. Res. Lett.,* **24,** 2589–2592.

Pierce, D., T. Barnett, and M. Latif, 2000: Connections between the Pacific Ocean Tropics and midlatitudes on decadal timescales. *J. Climate,* **13,** 1173–1194.

Rajagopolan, B., U. Lall, and M. Cane, 1997: Anomalous ENSO occurrences: An alternate view. *J. Climate,* **10,** 2351–2357.

Schneider, N., A. Miller, M. Alexander, C. Deser, and M. Latif, 1999a: Subduction of decadal North Pacific temperature anomalies: Observations and dynamics. *J. Phys. Oceanogr.,* **29,** 1056–1070.

——, S. Venzke, A. Miller, D. Pierce, T. Barnett, C. Deser, and M. Latif, 1999b: Pacific thermocline bridge revisisted. *Geophys. Res. Lett.,* **26,** 1329–1332.

Tanimoto, Y., N. Iwasaka, K. Hanawa, and Y. Toba, 1993: Characteristic variations of sea surface temperature with multiple time scales in the North Pacific. *J. Climate,* **6,** 1153–1160.

Trenberth, K. E., 1990: Recent observed interdecadal climate changes in the Northern Hemisphere. *Bull. Amer. Meteor. Soc.,* **71,** 993–998.

——, and J. Hurrell, 1994: Decadal atmosphere–ocean variations in the Pacific. *Climate. Dyn.,* **9,** 303–319.

——, and T. Hoar, 1996: The 1990–1995 El Niño-Southern Oscillation event: Longest on record. *Geophys. Res. Lett.,* **23,** 57–60.

Wang, C., and R. Weisberg, 1998: Climate variability of the coupled tropical–extratropical system. *Geophys. Res. Lett.,* **25,** 3979–3982.

Zhang, R., L. Rothstein, and A. Busalacchi, 1998: Origin of upper-ocean warming and El Niño changes on decadal scales in the tropical Pacific Ocean. *Nature,* **391,** 879–883.

Zhang, Y., J. Wallace, and N. Iwasaka, 1996: Is climate variability over the North Pacific a linear response to ENSO? *J. Climate,* **9,** 1468–1478.

——, ——, and D. Battisti, 1997: ENSO-like decade-to-century scale variability: 1900–93. *J. Climate,* **10,** 1004–1020.